Bol. Soc. Paran. Mat.
©SPM – E-ISSN-2175-1188
SPM: www.spm.uem.br/bspm

(3s.) **v. 2025 (43) 4** : 1–19.
ISSN-0037-8712
doi:10.5269/bspm.78525

Significance of Cross Diffusion on the Transient Behaviour of Radiating Casson Fluid near a Heated Slanted Plate*

M. Venkateswarlu†, M. B. Chennaiah and Md. Noor

ABSTRACT: High heat is used to destroy tumors and abnormal tissues through thermal ablation. The use of hyperthermia with chemotherapy and radiation therapy has been shown to increase their efficacy by damaging cancer cells and enhancing drug delivery. It is possible to use heat therapies to target tumors precisely while causing minimal damage to normal tissues at the same time. Diffusion thermo and thermo diffusion effects can affect local concentrations of therapeutic agents and heat transfer, potentially enhancing hyperthermia treatment effectiveness. The properties of Casson fluids, which intimately resemble blood motion in capillaries, are principally relevant in the design of biomedical devices such as artificial organs. A study of heat transfer in fluid flows can also assist in recognition of pollutant dispersion from technical sources and correcting combustion productivity for reducing transmission. The analysis presented here investigates the unsteady flow of Casson fluid across an impulsively initiated slanted plate, under the influence of thermo diffusion, diffusion thermo, and thermal radiation. In this study, the controlling flow equations are integrated adopting the Laplace transform mechanism, and the consequences emphasize concentration, temperature, and velocity distributions based on disparate parameter estimates. Tables analyze Sherwood number, Nusselt number, and skin friction factors. The consequences show that increasing the thermal radiation and plate inclination angle increases the fluid velocity, while decreasing the wall friction is found for opposing and assisting buoyancy forces. The Nusselt number and fluid temperature are increased by heat source and diffusion thermo effects. In a similar vein, the Sherwood number lowers with thermal radiation and rises with the thermo-diffusion effect.

Key Words: Heat source, diffusion thermo, thermal radiation, thermo diffusion, slanted plate.

Contents

1 Introduction 1

2 Mathematical Model 3

3 Exact Solution 5

4 Results and Discussion 9

5 Conclusions 15

6 Nomenclature 15

7 Appendix 16

1. Introduction

In the last few decades, researchers have made significant advances in studying how heat transfer and radiation affect fluid flows. Several applications of radiation from solar energy are popular worldwide, including solar distillation, solar vehicles, solar heaters, and solar turbines. Afaq et al. [1] discussed the effect of radiation on Casson fluid in an inclined magnetic field under a Forchhiemer porous medium. Reddy et al. [2] presented the heat loss and radiation cross-diffusion effects in viscous heating hydromagnetic Casson fluid in permeable vertical channel. Islam et al. [3] studied the flow of unsteady MHD Casson fluid through a cylindrical surface with effect of thermal radiation and chemical reactivity. In a triangular enclosure with thermal radiation and chemical reactions, MHD double-diffusive convection

* The project is partially supported by Siddhartha Academy of Higher Education, Vijayawada
† Corresponding author.
2010 *Mathematics Subject Classification:* 80A20, 85A25, 76RXX.
Submitted August 21, 2025. Published October 09, 2025

was performed by Kathyayani and Ramudu [4]. Rao et al. [5] informed that MHD Casson fluids behave differently over exponentially elongating sheets when it is subjected to thermal radiation and chemical boundary layer slip flow. In a magnetized radiative Casson fluid flow over a vertical stretching sheet, fractional analysis of thermo-diffusion and diffusion-thermo effects has been carried out by Zanib et al. [6]. Prakash et al. [7] reported the flow of a Casson fluid past a rotating porous medium with variable mass diffusion under thermal and radiation effects. Nisar et al. [8] studied the heat source/sink and thermal radiation in MHD Casson nanofluid peristaltic flow.

The energy unstableness brought on by transverse fluctuations in the concentration and temperature inclinations, along with the force potentiality that results become more complicated when double diffusion is added to fluid motion. The thermo diffusion effect is the instability in concentration caused by a temperature inclination, whereas the diffusion thermo effect is the instability in energy caused by a concentration inclination. In the fields of hydrology, isotope separation, geosciences, and the petroleum industry, the thermo diffusion and diffusion thermo effects are highly useful. Ilango and Lakshminarayana [9] explained the induced magnetic field and Soret-Dufour effects on viscous dissipative Casson liquid flow through porous medium over a stretching sheet. Sharma et al. [10] developed the melting, Soret and Dufour impression on MHD Casson liquid flow over a stretching sheet with slip conditions. Abbas et al. [11] presented the mathematical model of second-grade Casson fluid flow with Soret and Dufour impression over Riga sheet. Isa et al. [12] examined the velocity, temperature and concentration profiles for triple diffusive Casson fluid flow subjected to the Soret-Dufour parameters. Ramya and Deivanayaki [13] analyzed the impact of Soret and Dufour Effects on Casson Nano-liquid flow in a magnetic field along with heat and mass Transfer. Shah [14] presented the MHD orientation effects on Soret and Dufour phenomena in inclined corrugated triangular cavities with non-Newtonian liquids. Shankar and Sheri [15] discussed the unsteady MHD Casson fluid movement past a vertical plate in the vicinity of viscid dissipation and Dufour impressions. Patel [16] reported the Soret and heat generation effects on unsteady MHD Casson liquid flow in porous medium.

Many researchers have studied flow in slantwise configuration. The interpretation of fluid flow affected by physical strengths such as gravity-driven movement with nonzero impulses is being viewed for, especially in the research of heat transmission, e.g., solar collective mechanization. Rahman [17] examined the thermophoresis and Dufour-Soret contributions to MHD free convective heat and mass transfer in micropolar fluids with variable viscosity over an inclined quadratic stretching sheet. Palani and Naveen [18] addressed the comparative exploration of a magnetized power-law fluid past an inclined plate with variable physical properties. Kavitha and Angel [19] discussed the impact of rotation and chemical reactions on MHD mixed convection flow over an inclined heated porous plate with heat and mass transfer analysis. Njor et al. [20] addressed the irreversibility analysis of hydromagnetic Casson fluid flow through an inclined channel with isothermal boundary conditions.

The ongoing advancement in technology has prompted numerous studies on the fundamental principles of mass and heat transfer mechanisms, aiming to optimize and enhance various aspects of human being. Heat and mass and transmission perceptions are important in optimizing several scenarios and surroundings of living organisms explicitly for healthy lives. Sharma and Gorai [21] study magnetized Casson Nano-liquid flow over a porous surface with variable heat generation. Padma Devi et al. [22] reported the entropy generation in two-immiscible MHD flow of pulsating Casson fluid in a vertical porous space with slip effects. Patel and Patel [23] discussed the MHD bio-convection flow at Casson fluid stagnation point in porous medium: Cross-diffusion effect and heat production. Kumar et al. [24] addressed the heat and mass transfer on 3D radiative MHD Casson fluid flow over a stretching permeable sheet with chemical reaction and heat source/sink. Vinoth kumar and Poornima [25] developed the hybrid Casson magneto-convective rheological fluid flow from a horizontal circular cylinder under asymmetric heat generation/absorption. Patel et al. [26] reported the Soret and heat generation effects on unsteady MHD Casson fluid flow in porous medium. Reddy et al. [27] presented the unsteady absorption flow and dissipation heat transfer over a non-Newtonian fluid. Jagadha et al. [28] discussed the effect of higher order chemical reaction and Joule heating on rotational and permeable radiative MHD flow with heat generation/absorption.

The compact review of the literature survey defined that, the emanations of thermo diffusion and diffusion thermo in the perseverance of heat source and thermal radiation on unsteady Casson liquid flow

without magnetic field and porous medium navigating the inclined plate have not been included yet. This expedition is utilized in the processes of vaporization and condensation, isotope separation, the petrology industry, and containment movement in groundwater. This article seeks to analyze the behavior of an unsteady non-Newtonian Casson fluid flow under the importance of thermal radiation, heat source, thermo-diffusion and diffusion thermos effects, with time-varying concentration and temperature.

2. Mathematical Model

Imagine a viscous, radiative and incompressible Casson fluid flow across an infinite slanted surface that creates heat. In this article, variations in temperature and concentration are accounted for by diffusion thermo and thermal diffusion. There is a horizontal alignment of the $\bar{y}$-axis direction and a position of the plate along the $\bar{x}$-axis . Concentration of species and fluid temperature in the ambient environment are $\bar{C_w}$ and $\bar{T_w}$, respectively, but concentration and temperature levels in the far field are $\bar{C_\infty}$ and $\bar{T_\infty}$ respectively. At time $\bar{t} = 0$, the slanted plate and the liquid are motionless. For a time $\bar{t} > 0$, the surface starts with upward velocity $\bar{u_0}$ simultaneously varying the concentration levels as well as fluid temperature linearly with time. In addition, the liquid is characterized as gray, no scattering, but capable of both absorbing and emitting radiation. The surface is infinite and tilted at the angle α along the $\bar{x}$-axis, hence all the control components depends on $\bar{y}$ and $\bar{t}$ exactly. In Figure 1, we can see a physical illustration of this situation.

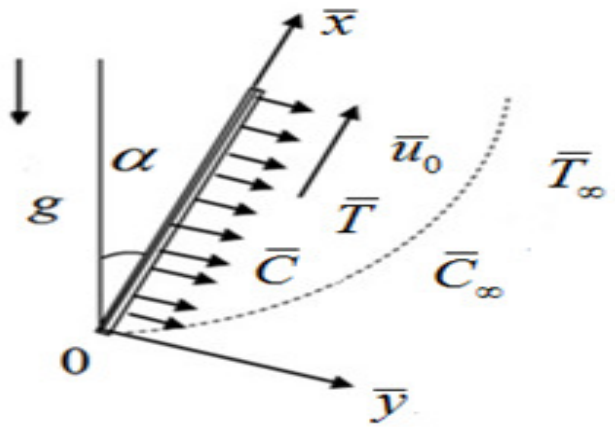

Figure 1: Depiction of a slanted plate

The Casson liquid's isotropic and non-compressible performance is characterized by the rheological expression declared as,

$$\tau_{ij} = \begin{cases} \left(2\mu_B + P_y\sqrt{\frac{2}{\pi}}\right)e_{ij}, \pi > \pi_c \\ \left(2\mu_B + P_y\sqrt{\frac{2}{\pi_c}}\right)e_{ij}, \pi < \pi_c \end{cases} \tag{2.1}$$

At this stage μ_B proclaim the liquid plastic dynamic viscosity, $P_y = \sqrt{2\pi}(\frac{\mu_B}{\beta})$ is the output reinforce of the liquid, π symbolize the product of deformations, especially $\pi = e_{ij}e_{ij}$ where e_{ij} is (i, j) th component of the deformity rate, andπ_c represents the crucial estimate of the product on the Casson liquid.

The expressions concerning the Casson fluid movement with Boussinesq simulation and analogous instructions through diffusion thermo and thermo diffusion repercussions can be stated as displayed below (See, Ref [29])

Continuity equation:

$$\frac{\partial \bar{v}}{\partial \bar{y}} = 0 \tag{2.2}$$

Momentum conservation equation:

$$\frac{\partial \bar{u}}{\partial \bar{t}} = \nu\left(1+\frac{1}{\beta}\right)\frac{\partial^2 \bar{u}}{\partial \bar{y}^2} + g\cos(\alpha)(\bar{T}-\bar{T}_\infty)\beta_T + g\cos(\alpha)(\bar{C}-\bar{C}_\infty)\beta_C \tag{2.3}$$

Energy conservation equation:

$$\frac{\partial \bar{T}}{\partial \bar{t}} = \frac{k_T}{\rho c_p}\frac{\partial^2 \bar{T}}{\partial \bar{y}^2} + \frac{Q_0(\bar{T}-\bar{T}_\infty)}{\rho c_p} - \frac{1}{\rho c_p}\frac{\partial q_r}{\partial \bar{y}} + \frac{D_m k_T}{c_s c_p}\frac{\partial^2 \bar{C}}{\partial \bar{y}^2} \tag{2.4}$$

Mass conservation equation:

$$\frac{\partial \bar{C}}{\partial \bar{t}} = D_m\frac{\partial^2 \bar{C}}{\partial \bar{y}^2} + \frac{D_m k_T}{T_m}\frac{\partial^2 \bar{T}}{\partial \bar{y}^2} \tag{2.5}$$

We can express the boundary and initial restrictions as displayed below

$$\left.\begin{array}{l} \bar{u}(\bar{y},0)=0, \bar{u}(0,\bar{t})=\bar{u}_0, \bar{u}(\infty,\bar{t})=0 \\ \bar{T}(\bar{y},0)=\bar{T}_\infty, \bar{T}(0,\bar{t})=\bar{T}_w, \bar{T}(\infty,\bar{t})=\bar{T}_\infty \\ \bar{C}(\bar{y},0)=\bar{C}_\infty, \bar{C}(0,\bar{t})=\bar{C}_w, \bar{C}(\infty,\bar{t})=\bar{C}_\infty \end{array}\right\} \tag{2.6}$$

The local radiative absorption for this type of gray fluid is described using the Rosseland approximation as follows

$$\frac{\partial q_r}{\partial \bar{y}} = -4\sigma_{sb} m_a(\bar{T}_\infty^4 - \bar{T}^4) \tag{2.7}$$

Here m_a and σ_{sb} signifies Stefan Boltzmann as well as mean absorption invariable respectively.

The temperature variation within the flow variation is under taking to be trivial so that $\bar{T}_\infty^4$ might be exhibited as a function of $\bar{T}$, there after applying Taylor's series procedure about $\bar{T}_\infty$. We have the result at the following after deserting superior order expressions

$$\bar{T}^4 \equiv \bar{T}_\infty^3(4\bar{T}-3\bar{T}_\infty) \tag{2.8}$$

By substituting the Eqs. (2.7) and (2.8) into Eq. (2.4), we acquired as

$$\frac{\partial \bar{T}}{\partial \bar{t}} = \frac{k_T}{\rho c_p}\frac{\partial^2 \bar{T}}{\partial \bar{y}^2} + \frac{Q_0(\bar{T}-\bar{T}_\infty)}{\rho c_p} - \frac{16\sigma_{sb} m_a \bar{T}_\infty^3(\bar{T}-\bar{T}_\infty)}{\rho c_p} + \frac{D_m k_T}{c_s c_p}\frac{\partial^2 \bar{C}}{\partial \bar{y}^2} \tag{2.9}$$

The successive dimensionless variables are initiated

$$\phi = \frac{\bar{C}-\bar{C}_\infty}{\bar{C}_w-\bar{C}_\infty}, \theta = \frac{\bar{T}-\bar{T}_\infty}{\bar{T}_w-\bar{T}_\infty}, U = \frac{\bar{u}}{\bar{u}_0}, \xi = \frac{\bar{y}\bar{u}_0}{\nu}, \tau = \frac{\bar{t}\bar{u}_0^2}{\nu} \tag{2.10}$$

Here we define $\bar{u}_0 = [g(\bar{T}_w-\bar{T}_\infty)\beta_T\nu]^{\frac{1}{3}}$ as the characteristic velocity (See, Ref [30]).

Eqs. (2.3), (2.5), and (2.9) resulting in a non-dimensional pattern

$$\frac{\partial U}{\partial \tau} - \left(1+\frac{1}{\beta}\right)\frac{\partial^2 U}{\partial \xi^2} = \theta\cos(\alpha) + N\phi\cos(\alpha) \tag{2.11}$$

$$\frac{\partial \theta}{\partial \tau} - \left(\frac{1}{\mathrm{Pr}}\right)\frac{\partial^2 \theta}{\partial \xi^2} + \left(\frac{R-H}{Pr}\right)\theta = \left(\frac{Dr}{Pr}\right)\frac{\partial^2 \phi}{\partial \xi^2} \tag{2.12}$$

$$\frac{\partial \phi}{\partial \tau} - \left(\frac{1}{Sc}\right)\frac{\partial^2 \phi}{\partial \xi^2} = \left(\frac{Sr}{Sc}\right)\frac{\partial^2 \theta}{\partial \xi^2} \tag{2.13}$$

Here $N = \frac{\beta_C(\bar{C}_w - \bar{C}_\infty)}{\beta_T(\bar{T}_w - \bar{T}_\infty)}$, $Dr = \frac{D_m(\bar{C}_w - \bar{C}_\infty)\rho}{c_s(\bar{T}_w - \bar{T}_\infty)}$, $Pr = \frac{c_p \nu \rho}{k_T}$, $Sr = \frac{k_T(\bar{T}_w - \bar{T}_\infty)}{T_m((\bar{C}_w - \bar{C}_\infty)}$, $H = \frac{Q_0 \nu^2}{k_T \bar{u}_0^2}$, $R_a = \frac{16\sigma_{sb} m_a \nu \bar{T}_\infty^3}{k_T}$, and $Sc = \frac{\nu}{D_m}$.

Consequently, we can write the initial and boundary restrictions as shown below:

$$\left.\begin{array}{l} U(\xi,0) = 0, U(0,\tau) = 1, U(\infty,\tau) = 0 \\ \theta(\xi,0) = 0, \theta(0,\tau) = 1, \theta(\infty,\tau) = 0 \\ \phi(\xi,0) = 0, \phi(0,\tau) = 1, \phi(\infty,\tau) = 0 \end{array}\right\} \tag{2.14}$$

Utilizing principles of Casson fluid dynamics, mass transfer, and heat transfer, shear strain τ_w , mass fluctuation j_w, and heat fluctuation q_w can be demonstrated as follows:

$$\tau_w = \mu(1 + \frac{1}{\beta})\left[\frac{\partial \bar{u}}{\partial \bar{y}}\right]_{\bar{y}=0} \tag{2.15}$$

$$q_w = -k_T\left[\frac{\partial \bar{T}}{\partial \bar{y}}\right]_{\bar{y}=0} \tag{2.16}$$

$$j_w = -D_m\left[\frac{\partial \bar{C}}{\partial \bar{y}}\right]_{\bar{y}=0} \tag{2.17}$$

In dimensionless pattern the coefficient of skin friction Cf , mass transmission coefficient Sh, and heat transmission coefficient Nu can be stated as

$$Cf = \frac{\tau_w}{\rho \bar{u}_0^2} \tag{2.18}$$

$$Nu = \frac{\nu}{\bar{u}_0}\frac{q_w}{(\bar{T}_w - \bar{T}_\infty)K_T} \tag{2.19}$$

$$Sh = \frac{\nu}{\bar{u}_0}\frac{j_w}{(\bar{C}_w - \bar{C}_\infty)D_m} \tag{2.20}$$

Utilizing the Eqs. (2.15) to (2.17) into Eqs. (2.18) to (2.20), we attained

$$Cf = \left(1 + \frac{1}{\beta}\right)\left[\frac{\partial U}{\partial \xi}\right]_{\xi=0} \tag{2.21}$$

$$Nu = -\left[\frac{\partial \theta}{\partial \xi}\right]_{\xi=0} \tag{2.22}$$

$$Sh = -\left[\frac{\partial \phi}{\partial \xi}\right]_{\xi=0} \tag{2.23}$$

3. Exact Solution

Decoupling Eqs. (2.11) - (2.13) requires a diminutive parameter$\epsilon << 1$ to obtain exact solutions (See, Ref [29])

$$U(\xi,\tau) = U_0(\xi,\tau) + \epsilon U_1(\xi,\tau) \tag{3.1}$$

$$\theta(\xi,\tau) = \theta_0(\xi,\tau) + \epsilon\theta_1(\xi,\tau) \tag{3.2}$$

$$\phi(\xi,\tau) = \phi_0(\xi,\tau) + \epsilon\phi_1(\xi,\tau) \tag{3.3}$$

On superseding Eqs. (3.1) - (3.3) into Eqs. (2.11) - (2.13), we gained

$$\frac{\partial U_0}{\partial \tau} - \left(1 + \frac{1}{\beta}\right)\frac{\partial^2 U_0}{\partial \xi^2} = \theta_0 \cos(\alpha) + N\phi_0 \cos(\alpha) \tag{3.4}$$

$$\frac{\partial\theta_0}{\partial\tau}-\left(\frac{1}{\mathrm{Pr}}\right)\frac{\partial^2\theta_0}{\partial\xi^2}+\left(\frac{R-H}{Pr}\right)\theta_0=0 \tag{3.5}$$

$$\frac{\partial\phi_0}{\partial\tau}-\left(\frac{1}{Sc}\right)\frac{\partial^2\phi_0}{\partial\xi^2}=0 \tag{3.6}$$

$$\frac{\partial U_1}{\partial\tau}-\left(1+\frac{1}{\beta}\right)\frac{\partial^2U_1}{\partial\xi^2}=\theta_1\cos(\alpha)+N\phi_1\cos(\alpha) \tag{3.7}$$

$$\frac{\partial\theta_1}{\partial\tau}-\left(\frac{1}{\mathrm{Pr}}\right)\frac{\partial^2\theta_1}{\partial\xi^2}+\left(\frac{R-H}{Pr}\right)\theta_1=\left(\frac{k}{Pr}\right)\frac{\partial^2\phi_0}{\partial\xi^2} \tag{3.8}$$

$$\frac{\partial\phi_1}{\partial\tau}-\left(\frac{1}{Sc}\right)\frac{\partial^2\phi_1}{\partial\xi^2}=\left(\frac{\lambda}{Sc}\right)\frac{\partial^2\theta_0}{\partial\xi^2} \tag{3.9}$$

Here $\lambda=\frac{Sr}{\epsilon}$ and $k=\frac{Dr}{\epsilon}$.

Consequently, we can write the initial and boundary restrictions as follows:

$$\left.\begin{array}{l}U_0(\xi,0)=0,U_0(0,\tau)=1,U_0(\infty,\tau)=0\\ \theta_0(\xi,0)=0,\theta_0(0,\tau)=1,\theta_0(\infty,\tau)=0\\ \phi_0(\xi,0)=0,\phi_0(0,\tau)=1,\phi_0(\infty,\tau)=0\end{array}\right\} \tag{3.10}$$

$$\left.\begin{array}{l}U_1(\xi,0)=0,U_1(0,\tau)=0,U_1(\infty,\tau)=0\\ \theta_1(\xi,0)=0,\theta_1(0,\tau)=0,\theta_1(\infty,\tau)=0\\ \phi_1(\xi,0)=0,\phi_1(0,\tau)=0,\phi_1(\infty,\tau)=0\end{array}\right\} \tag{3.11}$$

Utilizing the technique of Laplace transform, we solve Eqs. (3.4) - (3.9) regarding initial and boundary expressions in Eqs. (3.10) - (3.11).

Let $\eta=\frac{\xi}{2\sqrt{\tau}}$

In the next step, we transform Eqs. (3.4) to (3.9) into the pattern shown below

$$\frac{\partial U_0}{\partial\tau}-\left(\frac{\eta}{2\tau}\right)\frac{\partial U_0}{\partial\eta}-\left(1+\frac{1}{\beta}\right)\left(\frac{1}{4\tau}\right)\frac{\partial^2U_0}{\partial\eta^2}=\theta_0\cos(\alpha)+N\phi_0\cos(\alpha) \tag{3.12}$$

$$\frac{\partial\theta_0}{\partial\tau}-\left(\frac{\eta}{2\tau}\right)\frac{\partial\theta_0}{\partial\eta}-\left(\frac{1}{4Pr\tau}\right)\frac{\partial^2\theta_0}{\partial\eta^2}+\left(\frac{R-H}{Pr}\right)\theta_0=0 \tag{3.13}$$

$$\frac{\partial\phi_0}{\partial\tau}-\left(\frac{\eta}{2\tau}\right)\frac{\partial\phi_0}{\partial\eta}-\left(\frac{1}{4Pr\tau}\right)\frac{\partial^2\phi_0}{\partial\eta^2}=0 \tag{3.14}$$

$$\frac{\partial U_1}{\partial\tau}-\left(\frac{\eta}{2\tau}\right)\frac{\partial U_1}{\partial\eta}-\left(1+\frac{1}{\beta}\right)\left(\frac{1}{4\tau}\right)\frac{\partial^2U_1}{\partial\eta^2}=\theta_1\cos(\alpha)+N\phi_1\cos(\alpha) \tag{3.15}$$

$$\frac{\partial\theta_1}{\partial\tau}-\left(\frac{\eta}{2\tau}\right)\frac{\partial\theta_1}{\partial\eta}-\left(\frac{1}{4Pr\tau}\right)\frac{\partial^2\theta_1}{\partial\eta^2}+\left(\frac{R-H}{Pr}\right)\theta_1=\left(\frac{k}{4Pr\tau}\right)\frac{\partial^2\phi_0}{\partial\eta^2} \tag{3.16}$$

$$\frac{\partial\phi_1}{\partial\tau}-\left(\frac{\eta}{2\tau}\right)\frac{\partial\phi_1}{\partial\eta}-\left(\frac{1}{4Pr\tau}\right)\frac{\partial^2\phi_1}{\partial\eta^2}=\left(\frac{\lambda}{4Sc\tau}\right)\frac{\partial^2\theta_0}{\partial\eta^2} \tag{3.17}$$

Consequently, we can write the initial and boundary restrictions as shown below:

$$\left.\begin{array}{l}U_0(\eta,0)=0,U_0(0,\tau)=1,U_0(\infty,\tau)=0\\ \theta_0(\eta,0)=0,\theta_0(0,\tau)=1,\theta_0(\infty,\tau)=0\\ \phi_0(\eta,0)=0,\phi_0(0,\tau)=1,\phi_0(\infty,\tau)=0\end{array}\right\} \tag{3.18}$$

$$\left.\begin{array}{l}U_1(\eta,0)=0,U_1(0,\tau)=0,U_1(\infty,\tau)=0\\ \theta_1(\eta,0)=0,\theta_1(0,\tau)=0,\theta_1(\infty,\tau)=0\\ \phi_1(\eta,0)=0,\phi_1(0,\tau)=0,\phi_1(\infty,\tau)=0\end{array}\right\} \tag{3.19}$$

$$Cf = \left(1+\frac{1}{\beta}\right)\left(\frac{1}{2\sqrt{\tau}}\right)\left[\frac{\partial U}{\partial \eta}\right]_{\eta=0} \tag{3.20}$$

$$Nu = -\left(\frac{1}{2\sqrt{\tau}}\right)\left[\frac{\partial \theta}{\partial \eta}\right]_{\eta=0} \tag{3.21}$$

$$Sh = -\left(\frac{1}{2\sqrt{\tau}}\right)\left[\frac{\partial \phi}{\partial \eta}\right]_{\eta=0} \tag{3.22}$$

To find the exact solution, we can use Laplace transform.

$$\bar{U}(\eta, s) = \int_0^\infty \exp(-s\tau)U(\eta,\tau)\,d\tau \tag{3.23}$$

$$\bar{\theta}(\eta, s) = \int_0^\infty \exp(-s\tau)\theta(\eta,\tau)\,d\tau \tag{3.24}$$

$$\bar{\phi}(\eta, s) = \int_0^\infty \exp(-s\tau)\phi(\eta,\tau)\,d\tau \tag{3.25}$$

The solutions of Eqs. (3.12) - (3.17) regarding the initial and boundary expressions in Eqs. (3.18) - (3.19), are provided below

$$\begin{aligned} U_0(\eta,\tau) =& m_1\chi_1\left(0,\frac{1}{m_1},\eta,\tau\right) + m_2\exp(\tau m_4)\left[\chi_1\left(m_4,\frac{1}{m_1},\eta,\tau\right) - \chi_1\left(m_4+\frac{R-H}{Pr},Pr,\eta,\tau\right)\right] \\ &+ m_3\left[\chi_2\left(\frac{1}{m_1},\eta,\tau\right) - \chi_2\left(Sc,\eta,\tau\right)\right] + m_2\chi_1\left(\frac{R-H}{Pr},Pr,\eta,\tau\right) \end{aligned} \tag{3.26}$$

$$\theta_0(\eta,\tau) = \chi_1\left(\frac{R-H}{Pr},Pr,\eta,\tau\right) \tag{3.27}$$

$$\phi_0(\eta,\tau) = \chi_1\left(0,Sc,\eta,\tau\right) \tag{3.28}$$

$$\begin{aligned} U_1(\eta,\tau) =& m_{13}\exp(\tau m_4)\left[\chi_1\left(m_4+\frac{R-H}{Pr},Pr,\eta,\tau\right) - \chi_1\left(m_4,\frac{1}{m_1},\eta,\tau\right)\right] \\ &+ m_{14}\exp(\tau m_7)\chi_1\left(m_7,\frac{1}{m_1},\eta,\tau\right) - m_{15}\chi_1\left(0,\frac{1}{m_1},\eta,\tau\right) \\ &+ \lambda N m_9\left[\chi_2\left(\frac{1}{m_1},\eta,\tau\right) - \chi_2\left(Sc,\eta,\tau\right)\right] \\ &- m_{16}\exp(\tau m_7)\chi_1\left(m_7+\frac{R-H}{Pr},Pr,\eta,\tau\right) + m_{17}\chi_1\left(0,Sc,\eta,\tau\right) \\ &- m_{17}\exp(\tau m_7)\chi_1\left(m_1,Sc,\eta,\tau\right) - \lambda m_{12}N\chi_1\left(\frac{R-H}{Pr},Pr,\eta,\tau\right) \end{aligned} \tag{3.29}$$

$$\theta_1(\eta,\tau) = m_6 k\exp(\tau m_7)\left[\chi_1\left(m_7,Sc,\eta,\tau\right) - \chi_1\left(m_7+\frac{R-H}{Pr},Pr,\eta,\tau\right)\right] \tag{3.30}$$

$$\begin{aligned} \phi_1(\eta,\tau) =& m_6\lambda\exp(\tau m_7)\left[\chi_1\left(m_7,Sc,\eta,\tau\right) - \chi_1\left(m_7+\frac{R-H}{Pr},Pr,\eta,\tau\right)\right] \\ &+ \lambda\left[\chi_1\left(0,Sc,\eta,\tau\right) - \chi_1\left(\frac{R-H}{Pr},Pr,\eta,\tau\right)\right] \end{aligned} \tag{3.31}$$

The following is the simplified exact solution for fluid motion, fluid temperature, and species concentration

$$\begin{aligned}U(\eta,\tau) =& m_{23}\chi_1\left(0,\frac{1}{m_1},\eta,\tau\right)\\ &+ m_{24}\exp(\tau m_4)\left[\chi_1\left(m_4,\frac{1}{m_1},\eta,\tau\right)-\chi_1\left(m_4+\frac{R-H}{Pr},Pr,\eta,\tau\right)\right]\\ &+ m_{25}\left[\chi_2\left(\frac{1}{m_1},\eta,\tau\right)-\chi_2\left(Sc,\eta,\tau\right)\right]+m_{26}\chi_1\left(\frac{R-H}{Pr},Pr,\eta,\tau\right)\\ &+ m_{19}\exp(\tau m_7)\chi_1\left(m_7,\frac{1}{m_1},\eta,\tau\right)-m_{21}\exp(\tau m_7)\chi_1\left(m_7+\frac{R-H}{Pr},Pr,\eta,\tau\right)\\ &+ m_{22}\chi_1\left(0,Sc,\eta,\tau\right)-m_{22}\exp(\tau m_7)\chi_1\left(m_7,Sc,\eta,\tau\right)\end{aligned} \tag{3.32}$$

$$\begin{aligned}\theta(\eta,\tau) =& \chi_1\left(\frac{R-H}{Pr},Pr,\eta,\tau\right)\\ &+ Drm_6\exp(\tau m_7)\left[\chi_1\left(m_7,Sc,\eta,\tau\right)-\chi_1\left(m_7+\frac{R-H}{Pr},Pr,\eta,\tau\right)\right]\end{aligned} \tag{3.33}$$

$$\begin{aligned}\phi(\eta,\tau) =& \chi_1\left(0,,Sc,\eta,\tau\right)\\ &+ Srm_6\exp(\tau m_7)\left[\chi_1\left(m_7,Sc,\eta,\tau\right)-\chi_1\left(m_7+\frac{R-H}{Pr},Pr,\eta,\tau\right)\right]\\ &+ Sr\left[\chi_1\left(0,Sc,\eta,\tau\right)-\chi_1\left(\frac{R-H}{Pr},Pr,\eta,\tau\right)\right]\end{aligned} \tag{3.34}$$

3.1 Skin friction : The coefficient of skin friction can be stated by utilizing Casson fluid motion

$$\begin{aligned}Cf =& \left(1+\frac{1}{\beta}\right)\left[\left(\frac{m_{34}}{2\tau\sqrt{\pi}}+\frac{m_{36}}{\sqrt{\pi}}\right)+\frac{1}{2\sqrt{\tau}}\left[m_{35}\chi_3\left(m_4,0,\tau\right)+m_{37}\chi_3\left(0,\frac{R-H}{Pr},\tau\right)\right.\right.\\ &+ m_{38}\chi_3\left(m_4,\frac{R-H}{Pr},\tau\right)+m_{39}\chi_3\left(m_7,0,\tau\right)\\ &\left.\left.+ m_{40}\chi_3\left(m_7,\frac{R-H}{Pr},\tau\right)\right]\right]\end{aligned} \tag{3.35}$$

3.2 Coefficient of heat transfer: Heat transfer coefficient can be stated by utilizing Casson liquid energy transmission

$$Nu = -\frac{1}{2\sqrt{\tau}}\left[m_{31}\chi_3\left(m_7,\frac{R-H}{Pr},\tau\right)-m_{32}\chi_3\left(m_7,0,\tau\right)-\sqrt{Pr}\chi_3\left(0,\frac{R-H}{Pr},\tau\right)\right] \tag{3.36}$$

3.3 Coefficient of mass transfer: Mass transfer coefficient can be stated by utilizing Casson liquid mass transmission

$$\begin{aligned}Sh =& -\frac{1}{2\sqrt{\tau}}\left[m_{29}\chi_3\left(0,\frac{R-H}{Pr},\tau\right)+m_{30}\chi_3\left(m_7,\frac{R-H}{Pr},\tau\right)\right.\\ &\left.- m_{28}\chi_3\left(m_7,0,\tau\right)-m_{27}-\sqrt{\frac{Sc}{\pi\tau}}\right]\end{aligned} \tag{3.37}$$

Here the constants and functions are displayed in the Appendix.

4. Results and Discussion

We determine the direct interpretations of the deliberate predicament for particular values of key characterizing flow phenomenon such as the thermo diffusion parameter Sr, diffusion thermo parameter Dr, radiation parameter R, heat source parameter H, inclination angle α, and Casson fluid parameter β. The graphical plots are generated to examine the patterns of concentration ϕ, temperature θ, and liquid movement U based on the simulated data and used tables to compute the coefficient of skin friction Cf, coefficient of mass transfer Sh, as well as coefficient of heat transfer Nu. The buoyancy parameter $N = \frac{Gr}{Gm}$ is defined as the ratio of the thermal Grashof parameter to the solutal Grashof parameter. In this study, $N = -0.2$ coincide to opposing buoyancy force and $N = 0.2$ coincide to assisting buoyancy force. The numerical calculations are carried out imposing particular constant values for pertinent physical constraints $Sr = 0.3, Dr = 0.3, R = 0.5, H = 3, \alpha = \frac{\pi}{4}, \beta = 0.5, Pr = 0.71, Sc = 1$ and $\tau = 1$ which exercise to all plots and tables unless explicitly otherwise indicated. In the case of Casson fluid flow across a slanted plate, selecting the range for the Prandtl number is important because it represents the ratio of momentum diffusivity to thermal diffusivity. Here $Pr = 0.71$ is taken for air.

Figs. 2(a) and 2(b), display the manipulation of the thermo diffusion parameter Sr on the Casson liquid movement U in the proximity of opposing and assisting buoyancy forces. The thermo diffusion parameter specifies the donation of temperature inclination to mass dispersal in the liquid movement. Essentially, variations in temperature cause species to redistribute, leading to changes in liquid motion and concentration. It is identified that as the thermo diffusion parameter expands the fluid motion enhances in the vicinity of opposing buoyancy force and depletes in the vicinity of assistance buoyancy force. Figs. 3(a) and 3(b) depict the shape of the Casson liquid movement U in the proximity of opposing and assisting buoyancy forces with various estimates of the diffusion thermo parameter Dr. The diffusion thermo parameter demonstrates the benefaction of concentration inclination to hydroelectric power flux in the liquid movement. It shows how variations in temperature can drive mass flow in the fluid. It is recorded that as the diffusion thermo parameter escalates the Casson liquid movement diminishes in both cases. Hence there is a negative correlation between the Casson liquid movement and the diffusion thermo parameter. Furthermore, it has been observed that there is a significant variation in the influence of diffusion thermo parameters and thermo diffusion parameters on liquid movement.

Figs. 4(a) and 4(b) exemplify the results of the radiation parameter R on the liquid movement U in the vicinity of opposing and assisting buoyancy forces. In thermal radiation, electromagnetic waves are used to transfer heat. It affects a liquid's temperature and velocity when this occurs. Radiation parameters are used to measure this influence. Using these plots, it can be remarked that there is a practical swell in the Casson liquid movement in both cases with rising R values. Hence, the liquid movement is an increasing function of the thermal radiation parameter in both cases. In Figs. 5(a) and 5(b), we recognize that the heat source parameter H diminishes the Casson fluid motion U in the proximity of opposing and assisting buoyancy forces. There is a negative correlation between Casson fluid motion and the heat source parameter in both cases.

The disparities in the Casson liquid movement U for plate inclination angle α in the vicinity of opposing and assisting buoyancy forces are visible in Figs. 6(a) and 6(b). The inclination angle refers to the tilt of the plate relative to the flow direction. Changes in this angle affect how the fluid interacts with the plate's surface. Increasing the plate's inclination angle reduces the frictional force on the fluid near a non-magnetic field. The motion of the liquid becomes more pronounced in regions where opposing and supportive buoyancy forces converge, resulting in a greater angle of inclination. Therefore, an increased plate inclination angle reduces frictional forces, resulting in a significant increase in fluid velocity in both scenarios where there is no magnetic field and no porous medium present. It is displayed in Figs. 7(a) and 7(b) that, the liquid movement U decelerates with an enrichment of the non-Newtonian Casson parameter β in the vicinity of opposing and assisting buoyancy forces. Hence, increasing the Casson parameter grows the plasticity of the liquid, subsequently, diminishing the liquid transport. The liquid movement exhibits a decreasing trend as the Casson parameter increases in both scenarios.

Figs. 8(a) and 8(b) depict the influences of the diffusion thermo parameter Dr on the temperature profile θ and thermo diffusion parameter Sr on the concentration profile ϕ respectively. The liquid temperature and species concentration increases with escalating values of diffusion thermo parameter and thermo diffusion parameter. Figs. 9(a) and 9(b) display the impression of the heat source parameter

H on the temperature profile θ and concentration profile ϕ separately. The liquid temperature and concentration increase with higher values of the heat source parameter. The decreased incidence of the thermal radiation parameter R on the temperature and concentration profiles, respectively, visualized in Figs. 10(a) and 10(b). In both distributions, there is a perceived depreciation occasioned by an enlarged radiation parameter. In the real aspect, integrating R, the energy equation starts to restrain the thermal boundary layer, consequently, liquid temperature weakens, and the concentration retards. Additionally, it is noted that the heat source parameter and thermal radiation parameter have varying impacts on liquid temperature and concentration.

The computational variances in the skin friction, heat and mass transfer coefficients are displayed in tables 1 to 5 for dissimilar parameters. Tables 1 to 3 indicate that the skin friction coefficient is a measure of the resistance encountered by a liquid as it flows over a surface. The skin friction coefficient increases with the rise in Casson fluid parameter, diffusion thermo parameter, and heat source parameter near the opposing and assisting buoyancy forces. Whereas a reversal effect is apparent for increasing in inclination angle and thermal radiation parameter in the proximity of opposing and assisting buoyancy forces. The skin friction becomes weaker in the proximity of opposing buoyancy force and stronger in the proximity assisting buoyancy force with increasing values of thermo diffusion parameter. Table 4 indicates that the heat transfer coefficient increases with the diffusion thermo parameter and heat source parameter, while it decreases with the thermal radiation parameter. Table 5 indicates that the mass transfer coefficient increases with higher thermo diffusion parameters and heat source parameters, while a different trend is observed for the thermal radiation parameter.

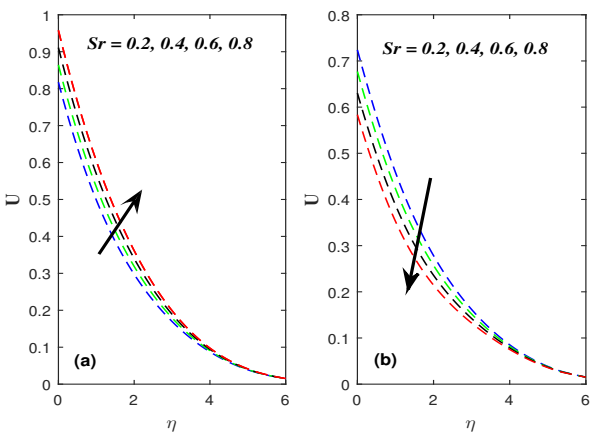

Figure 2: Depiction of Sr on U (a) Opposing buoyancy (b) Assisting buoyancy.

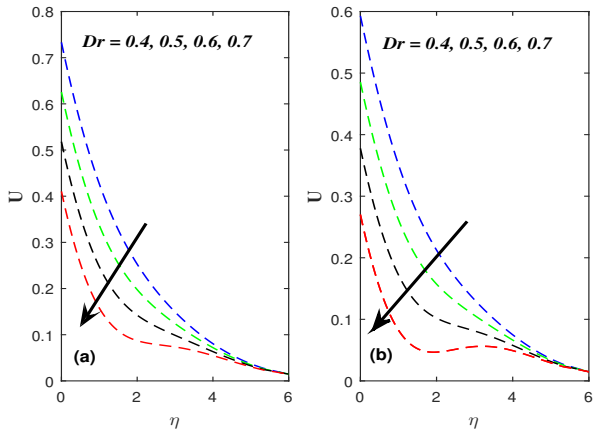

Figure 3: Depiction of Dr on U (a) Opposing buoyancy (b) Assisting buoyancy.

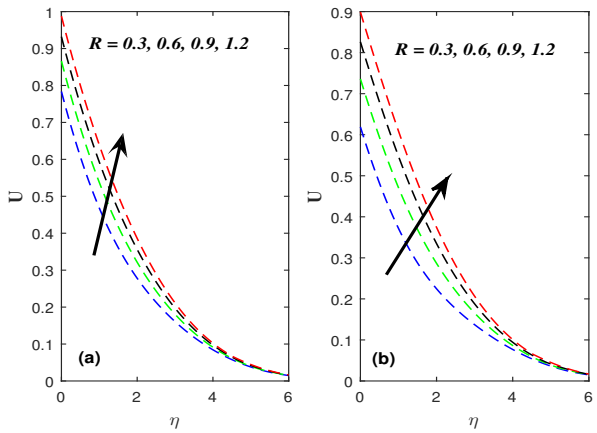

Figure 4: Depiction of R on U (a) Opposing buoyancy (b) Assisting buoyancy.

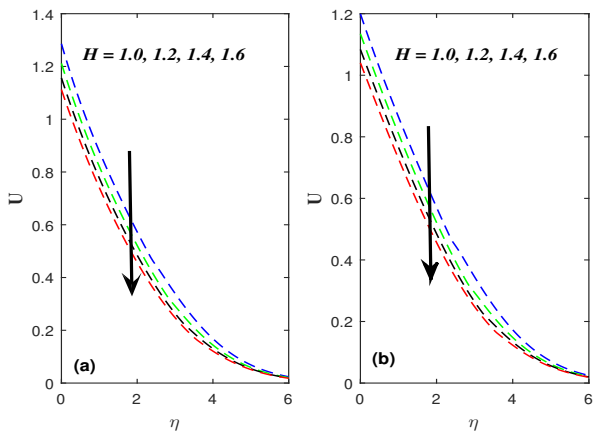

Figure 5: Depiction of H on U (a) Opposing buoyancy (b) Assisting buoyancy.

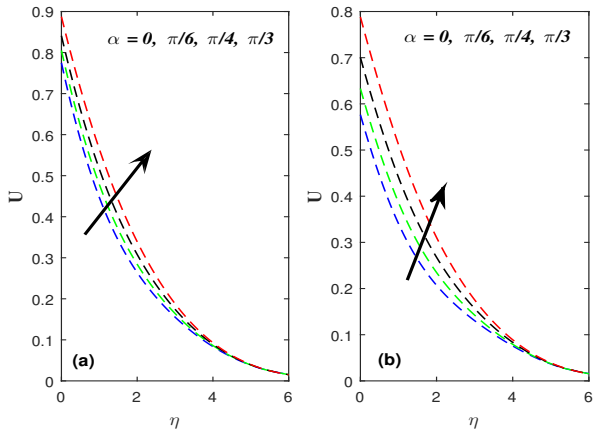

Figure 6: Depiction of α on U (a) Opposing buoyancy (b) Assisting buoyancy.

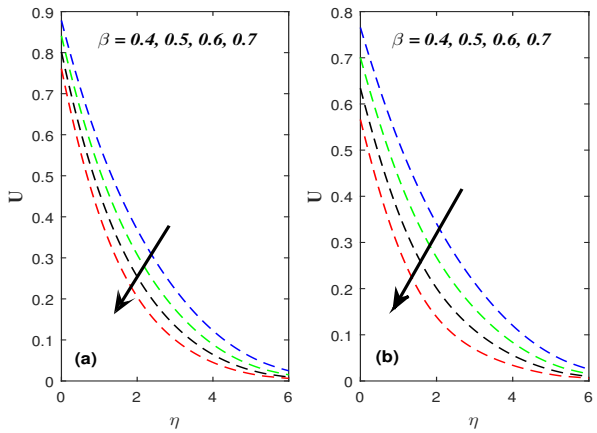

Figure 7: Depiction of β on U (a) Opposing buoyancy (b) Assisting buoyancy.

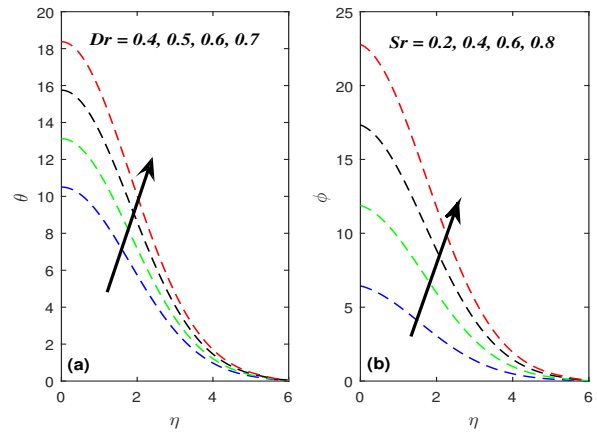

Figure 8: Depiction of (a) Dr on θ (b) Sr on ϕ.

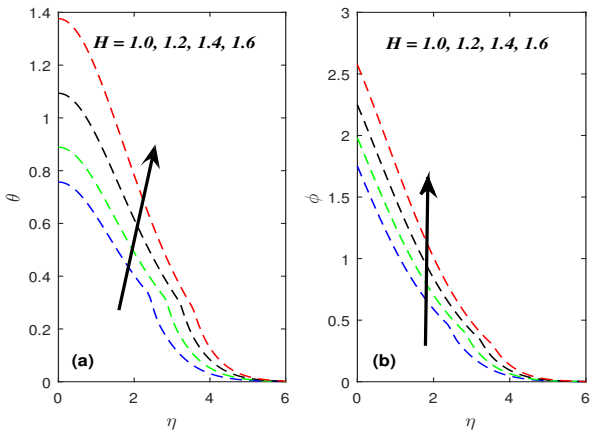

Figure 9: Depiction of (a) H on θ (b) H on ϕ.

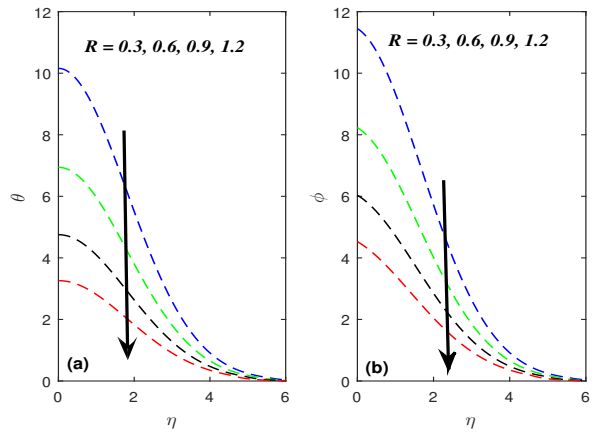

Figure 10: Depiction of (a) R on θ (b) R on ϕ.

Table 1: Variation of Cf with α and β.

		Cf	Cf
α	β	$N = -0.2$	$N = 0.2$
0	$\pi/4$	1.6508	1.9598
$\pi/6$	$\pi/4$	1.4935	1.7620
$\pi/4$	$\pi/4$	1.3072	1.5275
$\pi/3$	$\pi/4$	1.0650	1.2220
$\pi/4$	0.4	1.2568	1.5259
$\pi/4$	0.5	1.2984	1.5365
$\pi/4$	0.6	1.3451	1.5636
$\pi/4$	0.7	1.3950	1.6006

Table 2: Variation of Cf with Sr and Dr.

		Cf	Cf
Sr	Dr	$N = -0.2$	$N = 0.2$
0.2	0.3	1.3601	1.4737
0.4	0.3	1.2547	1.5814
0.6	0.3	1.1506	1.6897
0.8	0.3	1.0482	1.7985
0.3	0.4	1.6029	1.8264
0.3	0.5	1.9010	2.1266
0.3	0.6	2.2005	2.4276
0.3	0.7	2.5010	2.7291

Table 3: Variation of Cf with R and H.

		Cf	Cf
R	H	$N = -0.2$	$N = 0.2$
0.3	1.0	1.7892	2.2511
0.6	1.0	1.1463	1.2908
0.9	1.0	0.8819	0.9238
1.2	1.0	0.3345	0.5782
0.5	1.0	1.3072	1.5275
0.5	1.2	1.7892	2.2511
0.5	1.4	2.6544	3.5554
0.5	1.6	4.2489	5.9540

Table 4: Variation of Nu with Dr, R and H.

Dr	R	H	Nu
0.4	0.5	1.0	1.2449
0.5	0.5	1.0	1.6614
0.6	0.5	1.0	2.0808
0.7	0.5	1.0	2.5018
0.3	0.3	1.0	2.4600
0.3	0.6	1.0	0.4357
0.3	0.9	1.0	0.1565
0.3	1.2	1.0	0.2094
0.3	0.5	1.0	0.8362
0.3	0.5	1.2	2.4600
0.3	0.5	1.4	6.2009
0.3	0.5	1.6	14.4881

Table 5: Variation of Sh with Sr, R and H.

Sr	R	H	Sh
0.2	0.5	1.0	0.5646
0.4	0.5	1.0	1.4103
0.6	0.5	1.0	2.2560
0.8	0.5	1.0	3.1019
0.3	0.3	1.0	2.8329
0.3	0.6	1.0	0.4885
0.3	0.9	1.0	0.2201
0.3	1.2	1.0	0.2470
0.3	0.5	1.0	0.9874
0.3	0.5	1.2	2.8329
0.3	0.5	1.4	6.8534
0.3	0.5	1.6	15.5035

5. Conclusions

This article includes several important observations listed below:

- Increasing the diffusion thermo, heat source, and Casson liquid parameters slows liquid motion but raises skin friction for both opposing and assisting buoyancy forces.
- The augmentation of the thermal radiation parameter and the angle of inclination improve the fluid motion, while diminishing the skin friction coefficient for both opposing and assisting buoyancy forces.
- Increasing the thermo diffusion parameter enhances liquid motion when countering buoyancy force and reduces liquid motion when supporting buoyancy force.
- However, it decreases the coefficient of skin friction for opposing buoyancy force and increases it for assisting buoyancy force.
- Increasing the diffusion thermo parameter and heat source parameter enhances the temperature domain and heat transmission coefficient, but increasing the radiation parameter reduces the temperature domain and heat transmission coefficient.
- Increasing the thermo diffusion parameter and heat source parameter enhances the concentration domain and mass transmission coefficient, but increasing the radiation parameter reduces the concentration domain and mass transmission coefficient.
  The blood behaves differently than Newtonian liquids, especially at low shear rates. Since Casson liquid patterns capture blood's yield stress and viscosity behavior, they are highly relevant to studying blood flow near tumors. Heat source and thermal radiation directly relate to hyperthermia treatments, in which heat is delivered to tumors through external sources such as radiofrequency waves, microwaves, or lasers.

6. Nomenclature

g Acceleration due to gravity (ms^{-2})
$\bar{C}_\infty$ Uniform concentration
$\bar{C}$ Liquid species concentration
Cf Coefficient of skin friction
c_p Specific heat at constant pressure
c_s Concentration susceptibility
T_∞ Fluid Mean temperature
D_m Mass dispersal coefficient (m^2s^{-1})

k_T Fluid thermal conductivity $(Wm^{-1}K^{-1})$
H Non- dimensional heat consumption
Nu Coefficient of heat transfer
N Buoyancy ratio
Pr Prandtl number
R Radiation parameter
s Laplace Transform parameter
q_w Heat flux
Q_0 Dimensional heat generation
Sc Schmidt number
Sr Non-dimensional Soret number
Sh Coefficient of mass transfer
$\bar{t}$ Dimensional time (s)
$\bar{T}_\infty$ Uniform temperature (K)
$\bar{T}$ Temperature of the liquid (K)
U A scaled velocity (ms^{-1})
$\bar{u}$ Liquid velocity in $\bar{x}$ direction (ms^{-1})
$\bar{v}$ Liquid velocity in $\bar{y}$ direction (ms^{-1})
$\bar{u}_0$ Characteristic velocity (ms^{-1})

Greek symbols

α nclination angle (rad)
β_T Thermal extension coefficient
β_C Concentration extension coefficient
β Caisson fluid parameter
ρ Liquid density (Kgm^{-3})
ν Viscosity of the liquid (m^2s^{-1})
τ Dimensionless time (s)
ϕ A scaled concentration
θ A scaled temperature (K)
η A scaled coordinate (m)

7. Appendix

$$m_1 = 1 + \frac{1}{\beta}, m_2 = \frac{\cos\alpha}{m_1(R-H)}, m_3 = 1 - m_2, m_4 = \frac{m_1(R-H)}{m_1 Pr - 1}, m_5 = \frac{N\cos\alpha}{m_1 Sc - 1}, m_6 = \frac{Sc}{Pr - Sc},$$

$$m_7 = \frac{R-H}{Pr-Sc}, m_8 = \frac{\cos\alpha}{m_1 Pr - 1}, m_9 = \frac{\cos\alpha}{m_1 Sc - 1}, m_{10} = \frac{m_6 m_8}{m_4 - m_7}, m_{11} = \frac{m_6 m_9}{m_7}, m_{12} = \frac{m_8}{m_4},$$

$$m_{13} = (k + \lambda N)m_{10} + \lambda N m_{12}, m_{14} = (k + \lambda N)(m_{10} + m_{11}), m_{15} = m_{11}(k + \lambda N)m_{10} - \lambda N m_{12},$$

$$m_{16} = (k + \lambda N)m_{10}, m_{17} = (k + \lambda N)m_{11}, m_{18} = (Dr + NSr)m_{10} + NSr m_{12},$$

$$m_{19} = (Dr + NSr)(m_{10} + m_{11}), m_{20} = (Dr + NSr)m_{11} - NSr m_{12}, m_{21} = (Dr + NSr)m_{10},$$

$$m_{22} = (Dr + NSr)m_{11}, m_{23} = m_3 - m_{20}, m_{24} = m_2 - m_{18}, m_{25} = m_5 + NSr m_9,$$

$$m_{26} = m_2 - m_{12}NSr, m_{27} = Sr\sqrt{Sc}, m_{28} = m_{27}m_6, m_{29} = Sr\sqrt{Pr}, m_{30} = m_{29}m_6, m_{31} = m_6 Dr\sqrt{Pr},$$

$$m_{32} = m_6 Dr\sqrt{Sc}, m_{33} = (Dr + NSr)m_{10} + NSrm_{12}, m_{34} = \frac{m_{20} - m_3}{\sqrt{m_1}} - m_{22}\sqrt{Sc}, m_{35} = \frac{m_{18} - m_2}{\sqrt{m_1}}$$

$$m_{36} = (m_5 + m_9 NSr)\left(\sqrt{Sc} - \frac{1}{\sqrt{m_1}}\right), m_{37} = (m_{12}NSr - m_2)\sqrt{Pr}, m_{38} = (m_2 - m_{33})\sqrt{Pr},$$

$$m_{39} = m_{22}\sqrt{Sc} - \frac{m_{19}}{\sqrt{m_1}}, m_{40} = m_{21}\sqrt{Pr}, \delta_1 = \eta\sqrt{y} - \sqrt{\tau x}, \delta_2 = \eta\sqrt{y} + \sqrt{\tau x},$$

$$\chi_1(x, y, \eta, \tau) = \frac{1}{2}\left[erfc(\delta_1)\exp(-2\eta\sqrt{\tau xy}) + erfc(\delta_2)\exp(2\eta\sqrt{\tau xy})\right],$$

$$\chi_2(x, \eta, \tau) = (2\eta^2 x + 1)\tau erfc(\eta\sqrt{x}) - \frac{2\eta\sqrt{x}}{\sqrt{\pi}}\exp(-\eta^2 x),$$

$$\chi_3(x, y, \tau) = \sqrt{(x + y)}\exp(\tau x)erfc(\sqrt{\tau(x + y)}) + \frac{1}{\sqrt{\tau\pi}}\exp(-\tau x)$$

Acknowledgments

In appreciation of the reviewers' constructive comments and suggestions for enhancing the article, we acknowledge their assistance.

References

1. Afaq, H., Khan, M., Azhar, E., and Jamal, M., *Impact of radiation on Casson fluid in a Forchhiemer porous medium under inclined magnetic field*, Proceedings of the Institution of Mechanical Engineers, Part N: Journal of Nanomaterials, Nanoengineering and Nanosystems, 23977914251339238, (2025).

2. Reddy, B. P., Shamshuddin, M. D., Salawu, S. O., and Matao, M. P., *Cross-diffusion effects of viscous heating hydromagnetic Casson fluid flow in permeable vertical media with radiation and heat loss*, Partial Differential Equations in Applied Mathematics, 101225, (2025).

3. Islam, M. R., Hossain, M. A., and Alam, S. K., *Unsteady MHD Casson fluid flow through a cylindrical surface with effects of thermal radiation and chemical Reactivity*, Annals of Pure and Applied Mathematics, 31(1), 31-52, (2025).

4. Kathyayani, G., and Ramudu, G. V., *MHD double-diffusive convection of Casson fluid in a triangular enclosure with thermal radiation and chemical reactions*. Multiscale and Multidisciplinary Modeling, Experiments and Design, 8(6), 1-20, (2025).

5. Rao, A. S., Ganteda, C., Varalakshmi, M., Himabindu, I. B. N., Lakshmi, K. N. V., Prakash, G. B., and Almaliki, A. H., *The characteristics of thermal radiation and chemically boundary layer slip flow of a MHD Casson fluid over an exponentially elongating sheet*, Journal of Radiation Research and Applied Sciences, 18(2), 101504, (2025).

6. Zanib, S. A., Yaseen, L., Abbas, N., and Shatanawi, W., *Fractional analysis of thermo-diffusion and diffusion-thermo effects in a magnetized radiative casson fluid flow over a vertical stretching sheet*, Modeling Earth Systems and Environment, 11(4), 1-14, (2025).

7. Prakash, J., Selvaraj, A., Ragupathi, P., Al-Mdallal, Q. M., and Saranya, S., *Thermal and radiative effects on unsteady MHD flow of Casson fluid past a rotating porous medium with variable mass diffusion*, Case Studies in Thermal Engineering, 105865, (2025).

8. Nisar, Z., Muhammad, K., Aldosari, F. M., and Elseesy, I. E., *Peristaltic flow of MHD Casson nanofluid with heat source/sink and thermal radiation*, ZAMM-Journal of Applied Mathematics and Mechanics/Zeitschrift für Angewandte Mathematik und Mechanik, 105(1), e202300964, (2025).

9. Ilango, M. S., and Lakshminarayana, P., *Induced magnetic field and Soret–Dufour effects on viscous dissipative Casson fluid flow through porous medium over a stretching sheet*, Journal of Thermal Analysis and Calorimetry, 149(15), 8713-8727, (2024).

10. Sharma, S., Goyal, M., and Dadheech, A., *Melting, Soret and Dufour effect on MHD Casson fluid flow over a stretching sheet with slip conditions*, Journal of Engineering Mathematics, 146(1), 18, (2024).

11. Abbas, M. S., Shaheen, A., Abbas, N., and Shatanawi, W., *Mathematical model of second-grade Casson fluid flow with Soret and Dufour impact over Riga sheet*, Modern Physics Letters B, 38(25), 2450230, (2024).

12. Isa, S. S., Balakrishnan, N., Ismail, N. S., Arifin, N. M., and Ali, F. M., *The velocity, temperature and concentration profiles for triple diffusive Casson fluid flow subjected to the Soret-Dufour parameters*, CFD Lett., 16(3), 15-27,(2024).

13. Ramya, N., and Deivanayaki, M., *Impact of Soret and Dufour effects on Casson nanofluid flow in a magnetic field along with heat and mass transfer*, Indian Journal of Science and Technology, 18(13), 1059-1070, (2025).

14. Shah, S. S., *Magnetohydrodynamic orientation effects on Soret and Dufour phenomena in inclined corrugated triangular cavities with non-Newtonian fluids*, International Communications in Heat and Mass Transfer, 160, 108366, (2025).

15. Shankar, G., and Sheri, S. R., *Unsteady MHD Casson fluid flow past a vertical plate in the presence of viscid dissipation and Dufour effects* Multidiscipline Modeling in Materials and Structures, 21(2), 362-386, (2025).

16. Patel, H. R., *Soret and heat generation effects on unsteady MHD Casson fluid flow in porous medium*, Waves in Random and Complex Media, 35(1), 1172-1195, (2025).

17. Rahman, M. A., *Thermophoresis and Dufour-Soret contributions to MHD free convective heat and mass transfer in micropolar fluids with variable viscosity over an inclined quadratic stretching Sheet*, Annals of Pure and Applied Mathematics, 31(2), 89-106, (2025).

18. Palani, S., and Naveen, P., *A comparative exploration of a magnetized power-law fluid past an inclined plate with variable physical properties*, Sigma, 43(3), 827-834, (2025).

19. Kavitha, R., and Angel, J., *Impact of rotation and chemical reactions on MHD mixed convection flow over an inclined heated porous plate with heat and mass transfer analysis*, WSEAS Trans. Fluid Mech., 20, 40-50, (2025).

20. Njor, B. E., Lebelo, R. S., and Adesanya, S. O., *Irreversibility analysis of hydromagnetic Casson fluid flow through an inclined channel with isothermal boundary conditions*, Mathematics, 13(7), 1208, (2025).

21. Sharma, R. P., and Gorai, D., *Exploring the dynamics of magnetized Casson nanofluid flow across an extended porous surface with non-uniform heat generation*, Journal of Thermal Analysis and Calorimetry, 149(17), 9991-10002, (2024).

22. Padma Devi, M., Srinivas, S., and Vajravelu, K., *Entropy generation in two-immiscible MHD flow of pulsating Casson fluid in a vertical porous space with slip effects*, Journal of Thermal Analysis and Calorimetry, 149(14), 7449-7468, (2024).

23. Patel, S., and Patel, H. R., *Magnetohydrodynamics bio-convection flow at Casson fluid stagnation point in porous medium: Cross-diffusion effect and heat production*, Propulsion and Power Research, 13(3), 445-457, (2024).

24. Kumar, R., Khan, S., and Kumar, D. *Heat and mass transfer on 3D radiative MHD Casson fluid flow over a stretching permeable sheet with chemical reaction and heat source/sink*, Journal of Computational Analysis and Applications, 33(1), (2024).

25. Vinothkumar, B., and Poornima, T., *Hybrid Casson magneto-convective rheological fluid flow from a horizontal circular cylinder under asymmetric heat generation/absorption*, Journal of Thermal Analysis and Calorimetry, 149(13), 7071-7085, (2024).

26. Patel, H. R., *Soret and heat generation effects on unsteady MHD Casson fluid flow in porous medium*, Waves in Random and Complex Media, 35(1), 1172-1195, (2025).

27. Reddy, M. G., Krishnamurthy, M. R., Praveena, M. M., Naik, L. S., Prakasha, D. G., and Ganesh Kumar, K., *Unsteady absorption flow and dissipation heat transfer over a non-Newtonian fluid*, Waves in Random and Complex Media, 35(1), 2022-2036, (2025).

28. Jagadha, S., Gopal, D., Patil, N., Singh, S., Kishan, N., and Abhilasha, S. K., *Effect of higher order chemical reaction and Joule heating on rotational and permeable radiative MHD flow of Casson manganese ferrite fluid with heat generation/absorption*, Multiscale and Multidisciplinary Modeling, Experiments and Design, 8(3), 1-18, (2025).

29. Jha, B. K., and Gambo, Y. Y., *Unsteady free convection and mass transfer flow past an impulsively started vertical plate with Soret and Dufour effects: an analytical approach*, SN Applied Sciences 1, Article Number: 1234, (2019).

30. Turkyilmazoglu, M., and Pop, I., *Soret and heat source effects on the unsteady radiative MHD free convection flow from an impulsively started infinite vertical plate*, International Journal of Heat and Mass Transfer, 55, 7635-7644, (2012).

M.Venkateswarlu,
Department of Mathematics,
Siddhartha Academy of Higher Education,
Vijayawada, Andhra Pradesh, India.
E-mail address: mvsr2010@gmail.com

and

M. B. Chennaiah,
Department of Mechanical Engineering,
Siddhartha Academy of Higher Education,
Vijayawada, Andhra Pradesh, India
E-mail address: chennai303.mech@vrsiddhartha.ac.in

and

Md. Noor
Department of Mathematics,
Siddhartha Academy of Higher Education,
Vijayawada, Andhra Pradesh, India.
E-mail address: mdnoora0786@gmail.com